Dual-Species All-Optical Magnetometer Based on a Cs-K Hybrid Vapor Cell

Yudong Ding⊙, Wei Xiao⊙, Yixin Zhao⊙, Teng Wu, Xiang Peng⊙,*, and Hong Guo⊙†

State Key Laboratory of Advanced Optical Communication Systems and Networks, School of Electronics, and Center for Quantum Information Technology, Peking University, 100871 Beijing, China

We build and characterize a dual-species all-optical magnetometer based on a Cs-K hybrid vapor cell with a paraffin coating. Using the amplitude-modulated Bell-Bloom scheme and Faraday-rotation measurement, we show that the spin polarization of Cs and K atoms can be generated and detected independently. The noise floor of the Cs channel is 35 fT$/\sqrt{\text{Hz}}$, whereas that of the K channel is 260 fT$/\sqrt{\text{Hz}}$, which is affected mainly by the magnetic resonance broadening in the presence of mutual spin-exchange collisions. With use of the proposed device, *in situ* magnetic field stabilization is realized by use of (i) the K channel to monitor and compensate for the magnetic field noise and (ii) the Cs channel to read out the magnetic field after active stabilization. The low-frequency magnetic field noise can be suppressed by a factor of more than 1000 in the presence of magnetic field gradients. When applied to magnetic field stabilization, such *in situ* measurement is achieved more compactly and is more accurate than *ex situ* measurement that is realized with two spatially separated vapor cells. In addition, the proposed scheme could also be applied in a practical ground-surveying magnetometer based on dual working species.

I. INTRODUCTION

Optically pumped magnetometers based on alkali-metal atoms can measure magnetic fields with ultrahigh sensitivity and low power consumption [1,2], but they suffer from the nonlinear Zeeman effect [3]. The sensitivity and absolute measurement accuracy of such magnetometers are decreased by the broadening and splitting of the magnetic resonance lines, as well as by line-shape asymmetries. To avoid such decreased performance, a simple method is to use suitable alkali species for different ranges of the magnetic field [4]. For example, potassium magnetometers benefit from potassium's narrow and well-resolved magnetic resonance line under the terrestrial magnetic field [5,6], while cesium magnetometers perform well in a much weaker magnetic field (typically less than 40 μT), where the nonlinear Zeeman effect is not great [4,7]. However, use of two independent magnetometer sensors is likely to increase the system cost, and it is also difficult to guarantee identical magnetic field measurements if two spatially separated magnetic sensors are used in the presence of magnetic field gradients. An improved design involves implementing two independent alkali-metal (Cs and K) magnetometers in a single device with a single vapor cell, which enables flexible switching of the alkali-metal atoms to be used for different ranges of the magnetic field.

The proposed design also facilitates the simultaneous measurement of the spin precession of two species at the same position. Such *in situ* measurement [8,9] could be used for experimentally determining the intrinsic sensitivity of magnetometers [10] or for constructing new tandem magnetometers [11] or atomic comagnetometers [12]. In addition, *in situ* magnetic field stabilization could be realized by measuring the magnetic field noise with one species in the hybrid ensemble and generating an error signal to feedback-control the current in the magnetic field coils, and then the local magnetic field noise could be compensated and the magnetic field after stabilization could be read out by the other species. At the same time, a low-noise current is generated through active magnetic field stabilization and could be output for other applications, such as metrology or fundamental research [13–15]. *In situ* measurements of the magnetic field (current) are more accurate than *ex situ* measurements because magnetic gradients inevitably exist and decrease the consistency of measurements of the two species if they are spatially separated [7,16,17].

If two atomic species coexist in a single cell, then each atom will experience atomic collisions with atoms of its own species and the other species, among which spin-exchange (SE) collisions are dominant. Rapid SE collisions affect the transverse spin-relaxation time of atoms [18,19] and also transfer the spin polarization between different species [20–24]. To realize magnetometry based on hybrid ensembles, it is essential to begin by analyzing the SE effect. The rate of SE $R_{\text{SE}}^{A\text{-}B} = n_B \sigma_{\text{SE}}^{A\text{-}B} \bar{v}_T$ from atoms

---

*xiangpeng@pku.edu.cn
†hongguo@pku.edu.cn

of species A colliding with atoms of species B depends on the alkali-metal atomic density n_B, the alkali-alkali SE cross section $\sigma_{SE}^{A\text{-}B}$, and the average thermal velocity $\bar{v}_T$. Commonly, the saturated vapor densities of different alkali-metal species differ greatly at the same temperature [25]. Katz *et al.* [26] showed that in the SE-relaxation-free (SERF) regime [18,19], the minor species in the hybrid ensembles inherits the magnetic properties of the dominant species, including its transverse relaxation time (T_2), gyromagnetic ratio, and SERF magnetic field threshold. However, the magnetic properties of alkali-metal species in hybrid ensembles with the Bell-Bloom scheme [27] have not yet been studied systematically in other regimes in which the SE rate is relatively low and the bias magnetic field is not zero.

We report herein a dual-species all-optical magnetometer based on a Cs-K hybrid vapor cell with a paraffin coating. The spin precession of the Cs and K spins can be generated independently by use of the amplitude-modulated Bell-Bloom scheme and can be detected via Faraday-rotation measurements. We study theoretically and experimentally how SE collisions affect the magnetic properties of atomic spins in alkali-metal hybrid ensembles, including magnetic resonance broadening (related to T_2) and polarization transfer of both alkali species when they are exposed to magnetic fields. The noise floor of the K channel is higher than that of the Cs channel because of the K magnetic resonance broadening in the presence of mutual SE collisions within the hybrid cell. Furthermore, *in situ* magnetic field stabilization is realized in our scheme, in which the magnetic field is stabilized using the K channel and read out with the Cs channel at the same place in space and simultaneously in time. In comparison, spatially separated magnetic stabilization using independent paraffin-coated alkali atomic cells has a lower common-mode suppression ratio than magnetic stabilization using the hybrid cell in the presence of magnetic field gradients. We also discuss how to improve the overall performance of our design, as well as its potential magnetometer applications.

II. EXPERIMENTAL SETUP

Figure 1 shows the experimental setup. The paraffin-coated Cs-K vapor cell is spherical with a diameter of 25 mm. Two separate stems, each of length 20 mm, confine the ^{133}Cs atoms and K atoms with natural abundance; here, only ^{39}K atoms are considered because of their dominant abundance (93.2%). The vapor cell is placed in a Teflon oven that is heated by quad-twisted copper wires that carry a high-frequency heating current. The coating material is commercial paraffin wax, which has a melting temperature of $60\,^\circ$C, and we set the oven temperature to $45\,^\circ$C to increase the atomic vapor density in the hybrid cell (temperature is measured near the surface of the vapor
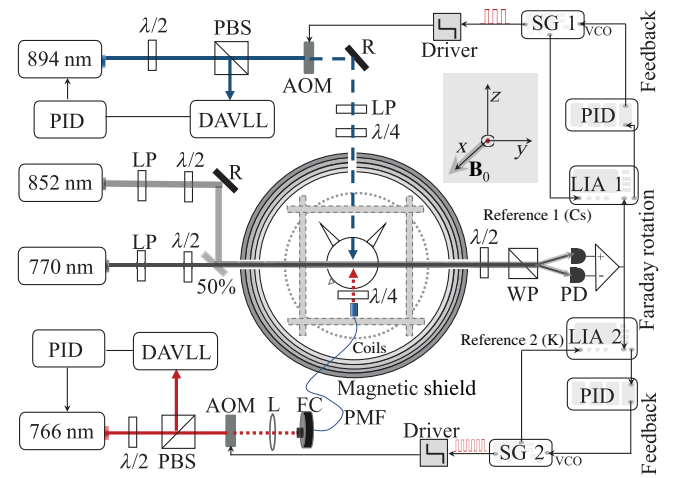

FIG. 1. Experimental setup of an all-optical Cs-K magnetometer. The bias magnetic field is along the axial direction of the magnetic shield and is perpendicular to the propagation direction of both the pump laser and the probe laser. AOM, acousto-optic modulator (which is used to modulate the pump beam); DAVLL, dichronic atomic vapor laser lock (which is used to lock the laser frequency); FC, fiber coupler; L, convex lens; LIA, lock-in amplifier; LP, linear polarizer; PBS, polarization beam splitter; PD, photodetector; PID, proportional-integral-derivative controller; PMF, polarization-maintaining fiber; R, reflector; SG, signal generator; VCO, voltage-controlled oscillator; WP, Wollaston prism; $\lambda/2$, half-wave plate; $\lambda/4$, quarter-wave plate; 50%, semitransparent and semireflective mirror.

cell). The oven is placed in a seven-layer magnetic shield made of 1-mm-thick high-permeability alloy, within which the magnetic field coils are driven with a current source (Krohn-Hite model 523) to generate a bias magnetic field in the x direction (along the axial direction of the magnetic shield and perpendicular to the propagation direction of both the pump laser and the probe laser).

To generate atomic spin polarization in the Cs-K vapor cell, two circularly polarized pump laser beams with frequencies resonant with the K D1 transition line at 770 nm (from $4^2S_{1/2}$ $F = 1$ to $4^2P_{1/2}$ $F' = 2$) and the Cs D1 transition line at 894 nm (from $6^2S_{1/2}$ $F = 3$ to $6^2P_{1/2}$ $F' = 4$), respectively, are transmitted in the z direction. We use a polarization-maintaining fiber and a fiber collimator to conduct the K laser beam into the magnetic shield, and all optical components within the shield are nonmagnetic. The intensities of the pump beams are modulated at the Larmor frequencies for Cs and K atoms, respectively, by our using acousto-optic modulators. The duty cycle of the modulation on the pump beam is set as 20%, and both laser beams have an average power of 35 μW ($1/e^2$ diameter of 2.8 mm). We detect the Faraday rotation of the probe beams to observe the spin behavior of each species. To reduce the absorption of the probe beams, their central frequencies are positively detuned by around 400 MHz from the Cs D2 transition line (from $6^2S_{1/2}$ $F = 4$ to $6^2P_{3/2}$ $F' = 5$)

and by around 200 MHz from the K D2 transition line (from $4^2S_{1/2}$ $F = 2$ to $4^2P_{3/2}$ $F' = 3$). These probe beams propagate in the y direction and are combined with a semitransparent and semireflective mirror.

The spin polarization of each species is measured with a polarimeter and is demodulated by use of a lock-in amplifier (LIA). Here, two independent LIAs are referred to the Cs and K pump laser modulations, respectively, in which the time constant is set as 300 µs and the order of the filter is set as 2 for the output. In addition, we operate the Cs (K) Bell-Bloom magnetometer in the closed-loop mode to increase the bandwidth, where the voltage-controlled oscillator of the signal generator is locked to the atomic resonance with a proportional-integral-derivative (PID) controller.

III. RESULTS AND DISCUSSION

A. Sensitivity

Figure 2 shows the noise floor of the Cs channel and the K channel, respectively. During the test, the hybrid cell is immersed in the bias magnetic field, which is generated using the current source and the magnetic coil with a constant of 40 nT/mA. The bias magnetic field is generated for the Bell-Bloom magnetometer's normal operation, which inevitably introduces electrical noise associated with the current-source noise. Here, the bias magnetic field is set as 0.3 µT to reduce the effect of the magnetic field noise because the commercial current source has a lower noise level with a small current output (less than 10 mA). In addition, the magnetic field gradients have much less effect on the magnetic resonance spectrum of each species when a small magnetic field is applied. The noise floor measured with the Cs channel using the hybrid cell is 35 fT/$\sqrt{\text{Hz}}$, whereas that measured with the K channel is 260 fT/$\sqrt{\text{Hz}}$,
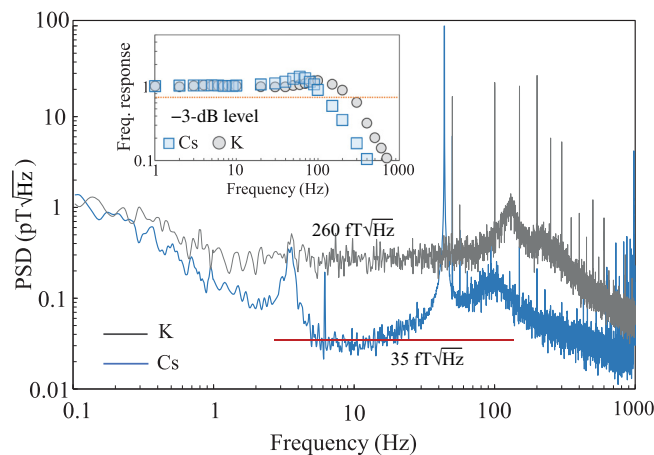

FIG. 2. Power spectral density (PSD) of magnetic field noise measured with the Cs channel (blue line) and the K channel (gray line) in our design. The inset shows the signal frequency responses.

as shown in Fig. 2. As the magnetic field noise contributed by the current source is the same for each channel in theory, the noise floor of 260 fT/$\sqrt{\text{Hz}}$ in the K channel is contributed mainly by its intrinsic noise. The use of independent laser sources and electronic devices and the differences in the magnetic resonance spectra of K and Cs atoms cause the two channels to differ not only in the noise floor but also in some of the industrial frequency noise at given frequencies, in which case the noise of the bias magnetic field (current) is no longer the dominant noise source for the two measuring channels.

Here, both measuring channels are operated in the closed-loop mode to extend their bandwidths. Frequency responses of each channel are measured by our applying an oscillating magnetic field of 1.5 nT (peak to peak) at different frequencies. The bandwidths (corresponding to the frequency where the signal amplitude is 3 dB smaller than that of the low-frequency limit) are approximately 100 Hz for the Cs channel and 200 Hz for the K channel. Operating Bell-Bloom magnetometers in closed-loop mode allows the bandwidth to be expanded beyond the magnetic resonance linewidth, but also necessarily results in an increase of the noise outside the original magnetic resonance linewidth and leads to a larger response at higher frequencies just before the cut frequency. The conditions to achieve a flat spectral response depend on the detuning between the Larmor-precession frequency and the optical-modulation frequency [28,29] and the PID controller parameters for closed-loop operation [7,30,31].

We also compare the noise floor of the two measuring channels of our design with that of Bell-Bloom magnetometers that are based on a pure K (Cs) vapor cell. The noise floor of the Cs channel is close to that of the Cs magnetometer using a pure Cs vapor cell, which shares exactly the same experimental scheme, laser source, and electronic equipment [32]. However, the noise floor measured with the K channel is much greater than that of the K magnetometer using a pure K vapor cell. The intrinsic noise floor of Bell-Bloom K magnetometer using a pure K cell is 30 fT/$\sqrt{\text{Hz}}$, which is measured under exactly the same experimental conditions [33]. On the basis of this finding, it is believed that the presence of Cs atoms in the hybrid vapor cell is the main cause of the sensitivity decrease of the K channel.

B. Magnetic-resonance-linewidth broadening

The sensitivity of atomic magnetometers benefits from a narrow magnetic resonance linewidth. The Cs and K magnetic resonance signals are measured within the magnetic shield and under the bias magnetic field of 0.3 µT to reduce the broadening effects that are caused by the magnetic field gradients and the nonlinear Zeeman effect. During the measurement, the in-phase and quadrature components of magnetic resonance signals are continuously read out and

recorded from LIAs while the modulation frequency of the pump laser is scanned near the Larmor frequency of K (Cs) atoms under the bias magnetic field.

Figure 3(a) shows the measurement of the Cs (K) magnetic resonance linewidth using the hybrid cell, while, for comparison, the pure Cs or K cell with a paraffin coating (cylinder, length of 3 cm, diameter of 2.5 cm) is tested under a similar experimental setup. With an increased cell temperature, the magnetic resonance linewidth of Cs atoms in the hybrid cell [orange circles in Fig. 3(a)] and the magnetic resonance linewidth of Cs atoms in the pure Cs cell [gray squares in Fig. 3(a)] have similar broadening trends. However, as shown in Fig. 3(b), the difference between the K magnetic resonance linewidth measured with the hybrid cell (blue circles) and that measured with the pure K cell (red squares) is obvious.

In the hybrid cell, the saturated vapor densities of different alkali-metal species differ greatly at the same temperature [25,34]; for example, the Cs vapor density n_{Cs} is about 60 times larger than the K vapor density n_K at a temperature of 45 °C. Therefore, the SE rate experienced by the K species in the hybrid ensembles is determined predominantly by collisions with the Cs species, whereas the Cs species is affected only weakly by the presence of the K species, which could account for the similar broadening trend of the Cs magnetic resonance spectrum in the hybrid cell and the Cs magnetic resonance spectrum in the pure Cs cell. On the other hand, the K magnetic resonance spectrum undergoes significant linewidth broadening in the hybrid cell mainly because of the mutual SE
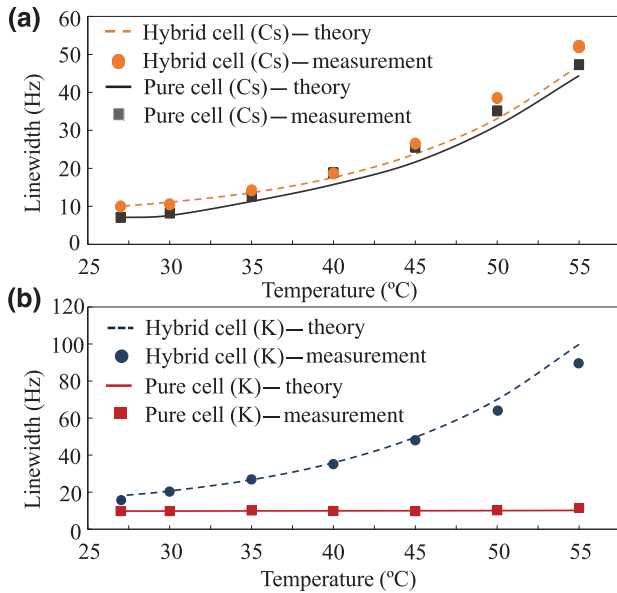

FIG. 3. Simulation and measurement of (a) Cs magnetic resonance linewidth using the hybrid cell (orange) and a pure Cs cell (gray) and (b) K magnetic resonance linewidth using the hybrid cell (blue) and a pure K cell (red).

collisions with Cs atoms. For pure K vapors, the magnetic resonance linewidth is less sensitive to the cell temperature because of the relatively low K atomic density, in which case the SE-collision-induced linewidth broadening is not dominant.

To determine the mechanism for linewidth broadening and verify the experimental results, we use a general model to study systematically how SE collisions affect the behavior of atomic spins in alkali-metal hybrid ensembles. The model is based on the modified Bloch equations derived from the density-matrix equation in a low-spin-polarization limit [18,33,35]. In our scheme, neither the Cs channel nor the K channel works under the SERF regime. The frequencies of the pump and probe lasers are chosen to generate and detect the polarization of a certain ground-state hyperfine level of each species ($F = 2$ for K atoms and $F = 4$ for Cs atoms). The spin relaxation due to SE collisions is different for each alkali-species hyperfine level in the hybrid ensembles, which depends on their experienced SE rate and the broadening coefficients related to the nuclear spin I_S. According to the model, the Cs magnetic resonance broadening caused by the SE collisions is described as

$$\Gamma_a^{Cs} = \frac{7}{32} R_{SE}^{Cs\text{-}Cs}, \quad \Gamma_b^{Cs} = \frac{15}{32} R_{SE}^{Cs\text{-}Cs}, \quad (1)$$

where Γ_a^{Cs} and Γ_b^{Cs} are the magnetic resonance linewidths of Cs hyperfine level a and Cs hyperfine level b ($a = I_S + 1/2$ denotes the higher hyperfine level and $b = I_S - 1/2$ denotes the lower one), respectively. The SE collisions experienced by Cs atoms with other Cs atoms are dominant because $R_{SE}^{Cs\text{-}Cs} \gg R_{SE}^{Cs\text{-}K}$. The broadening coefficients are derived and depend on the nuclear spin I_S ($I_S = 7/2$ for Cs), as given in Supplemental Material [36]. Similarly, the K magnetic resonance broadening caused by SE collisions can also be obtained and is given as

$$\Gamma_a^K = \frac{7}{16} R_{SE}^{K\text{-}Cs}, \quad \Gamma_b^K = \frac{11}{16} R_{SE}^{K\text{-}Cs}, \quad (2)$$

where Γ_a^K and Γ_b^K are the magnetic resonance linewidths of K hyperfine level a and K hyperfine level b, respectively. The mutual SE collisions are the dominant collisional interaction for K atoms because $R_{SE}^{K\text{-}Cs} \gg R_{SE}^{K\text{-}K}$. Here, the broadening coefficients are determined by a coupling-interaction matrix, as given in Supplemental Material [36].

The SE-collision rate R_{SE} is given by $R_{SE}^{K\text{-}Cs} = n_{Cs} \sigma_{SE}^{K\text{-}Cs} \bar{v}_T$ and $R_{SE}^{Cs\text{-}Cs} = n_{Cs} \sigma_{SE}^{Cs\text{-}Cs} \bar{v}'_T$. The SE cross section can be found in Ref. [37,38]. Here $\bar{v}_T$ and $\bar{v}'_T$ are the average thermal velocity of K atoms and Cs atoms, respectively, and can be determined by the atomic mass and the ambient temperature. There is no individual temperature control for the two stems of the hybrid cell, so the temperature that determines the vapor density in the cell body is

the same for Cs and K atoms. On the basis of these determined parameters, we numerically simulate the magnetic resonance linewidth of K or Cs atoms (see Supplemental Material [36] for a more-detailed calculation). Figure 3 shows the simulated magnetic resonance broadening (solid line) for each species. The trends in the theoretical calculations agree with those in the experimental measurements. It should be noted that the temperature dependence of magnetic resonance broadening induced by such spin-destruction collisions or the laser power is ignored because the broadening changes only slightly with an increase in temperature when compared with the broadening due to SE collisions.

The broadened K magnetic resonance linewidth in the hybrid cell is the main cause of the decrease of the sensitivity of the K channel since the sensitivity is proportional to the total resonance linewidth divided by the signal-to-noise ratio [39]. Compared with the pure K cell, the broadening of the magnetic-resonance-spectrum linewidth in the hybrid cell increases by about 5 times under a similar experimental setup and the signal-to-noise ratio of the magnetic resonance signal also decreases.

C. Transfer of transverse spin polarization through spin-exchange collisions

In addition to the magnetic-resonance-broadening effect, SE collisions cause the transfer of spin polarization between the two alkali species as well, which can affect the independent measurement of the spin polarization of each species. In our scheme, the spin polarization of each species is generated in the transverse direction (i.e., perpendicular to the direction of the magnetic field), and the transfer of transverse spin polarization happens naturally when the A atoms and the B atoms have the same g factor (e.g., ^{39}K and ^{87}Rb) because the Larmor precessions of the two species are synchronous [40]. By contrast, if the A atoms and the B atoms have different g factors, the transverse spin polarization that is transferred successively from atoms of the other species cannot accumulate because of the different Larmor frequencies [22]. However, the transfer of polarization cannot be ignored under relatively small magnetic fields because the difference in the Larmor frequencies of the two species $(\gamma_K - \gamma_{Cs})B_0$ is smaller than the magnetic resonance linewidth of each species, where γ_K and γ_{Cs} are the gyromagnetic ratios of the K atoms and the Cs atoms, respectively.

To detect the transfer of transverse spin polarization in the hybrid cell, we optically polarize one of the alkali-metal species and detect the polarization of the other species. Currently, the spin polarization that is transferred from the K atoms to the Cs atoms can be ignored because of the relatively low mutual SE rate experienced by the Cs atoms, and thus we focus on the transfer of spin polarization from the Cs atoms to the K atoms. Here, the Cs

atoms are polarized with the Cs-D1-line laser and the K atoms are detected with the K-D2-line laser, as shown in the inset in Fig. 4. The transverse spin polarization of K atoms is determined by our extracting the amplitude component of the K Faraday-rotation signal with LIA 1. During the experiments, the Cs probe laser beam is blocked.

With increased bias magnetic field, the transverse spin polarization of K atoms generated through spin transfer has an inversely proportional deceasing trend, as shown in Fig. 4. The experimental results can be explained by use of the model of synchronized optical pumping and the Bloch equation [41]. When a relatively large bias magnetic field is applied, i.e., $(\gamma_K - \gamma_{Cs})B_0$ is far larger than the mutual SE rate and the magnetic resonance linewidth of two species, the transfer between the spin polarization of two species in the Bell-Bloom scheme can be ignored. See the more-detailed analysis in Supplemental Material [36]. In addition, the polarized K and Cs atoms will generate magnetic fields, which could reach the order of nanoteslas [42]. However, because the proposed Bell-Bloom magnetometers generate transverse polarization, which is perpendicular to the bias magnetic field, the magnetic field generated by polarized atoms adds in quadrature to the bias magnetic field, which can be ignored when a relatively large magnetic field is applied [7].

Although the polarization transfer is hopefully avoided in our design, use of the efficient polarization transfer can be considered to suppress the light shift of hybrid species by indirect optical pumping [21,43] and increase the spin polarization of the target atoms [24,44–47]. In these applications, hybrid vapor cells with buffer gas are commonly used instead of vapor cells with an antirelaxation coating because of the need for high cell temperatures to achieve high rates of SE collisions between different species.
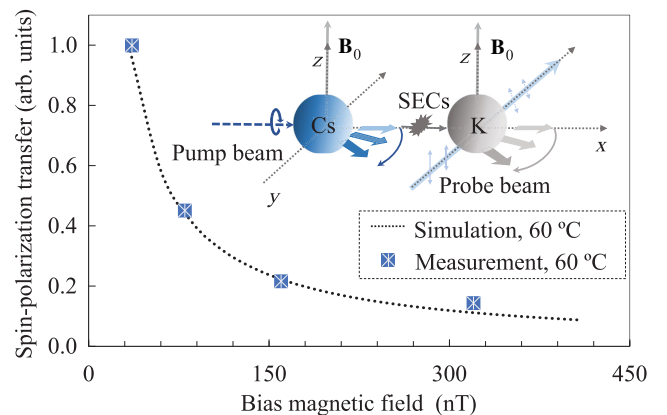

FIG. 4.   Simulated and measured dependence of transfer of transverse spin polarization on the bias magnetic field. The transfer of spin polarization is detected by our optically pumping the Cs atoms and measuring the Faraday rotation of the K atoms. SEC, spin-exchange collision.

IV. *IN SITU* MAGNETIC FIELD STABILIZATION

On the basis of the design of the dual-species magnetometer with a single hybrid vapor cell, we present the application of *in situ* magnetic field stabilization. The feedback loop for active magnetic field stabilization is shown in Fig. 5(a). The bias magnetic field B_C is generated with magnetic field coils, which are driven by a voltage-controlled current source. The magnetic field measurement of the K stabilization channel is compared with the reference to generate an error signal. To zero the error signal, a feedback signal is produced to dynamically control the current in the magnetic field coils through the voltage-controlled current source. The magnetic field noise is read out with the Cs channel. Figure 5(b) shows the magnetic field noise before and after active magnetic field stabilization. Here, the coil constant is 130 nT/mA and the bias magnetic field is set at 25 µT. When the apparatus works in the open-loop mode, the uncompensated magnetic field noise (peak-to-peak noise at 0.1–1 Hz) is 980 pT, which is typically dominated by the current-conversion magnetic field noise. When the apparatus operates in the closed-loop mode, the magnetic field noise is suppressed and the peak-to-peak noise at 0.1–1 Hz is suppressed to 5.6 pT. As the magnetic field noise is dominated by the current-source noise, the current-source noise

is suppressed synchronously through the magnetic field stabilization.

The performance calibration of magnetic field stabilization is determined mainly by the ability to reject common-mode noise [7,16], which might degrade in the presence of magnetic field gradients. The results for magnetic field stabilization in the time domain with use of the hybrid vapor cell and two independent vapor cells are compared in Fig. 5(c). The independent Cs cell with a paraffin coating is placed in the center of the magnetic shield, and spatial laser beams as introduced in Sec. II are used. An integrated K magnetic sensor with the independent paraffin-coated K cell is placed near the Cs vapor cell at a distance of 5 cm. The central axis of the two independent cells coincides with the *z* axis of the magnetic coils. A sinusoidal test field with a frequency of 0.01 Hz and an amplitude of 8000 pT (peak-to-peak value) is generated to characterize the magnetic-field-noise suppression in the time domain. When the test field is stabilized and detected by the two independent vapor cells, the measurement of the Cs channel has a peak-to-peak noise of 220 pT in the time domain. For comparison, when the Cs-K hybrid vapor cell is used, the peak-to-peak noise after magnetic field stabilization is suppressed to 6.3 pT. The suppression ratio of the test field reaches more than 1000. The *in situ* stabilization increases
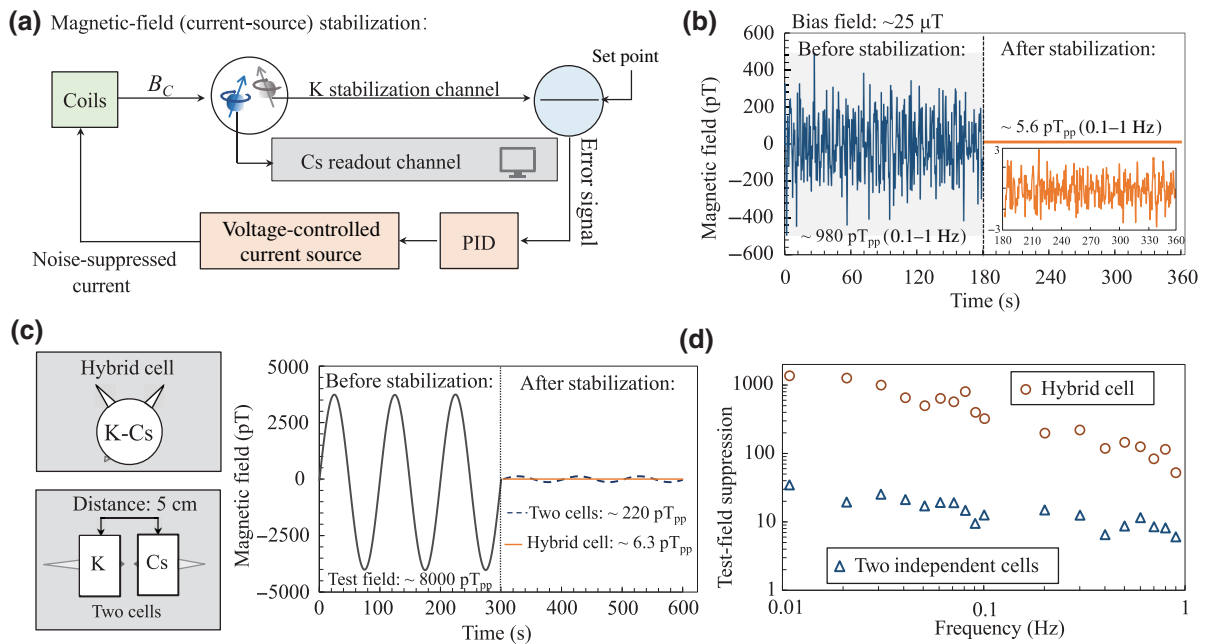

FIG. 5. (a) Experimental scheme of active magnetic field (current-source) stabilization with a Cs-K all-optical magnetometer. Here, the K channel is used to measure and compensate for the magnetic field noise, while the Cs channel is used to read out the noise-suppressed magnetic field. B_C is the magnetic field that generated by the magnetic field coils. (b) Magnetic field noise measured before and after *in situ* magnetic field stabilization; the bias magnetic field is 25 µT. (c) Sinusoidal test field (gray line) with a frequency of 0.01 Hz and an amplitude of 8000 pT (peak-to-peak value) generated to characterize the magnetic-field-noise suppression in the time domain. The orange line (blue line) represents the magnetic field measurement after active stabilization using the hybrid cell (independent Cs and K cells). (d) Frequency dependence of test-field suppression in active magnetic field stabilization.

the test-field suppression, mainly due to its greater suppression effect on the test-field gradients. Similarly, we also test the stabilization of the test field with different frequencies, as shown in Fig. 5(d). With increase of the frequency, the test-field suppression ratio decreases because the feedback system has a limited bandwidth and cannot respond to and compensate for high-frequency magnetic-field disturbances. Fortunately, by setting suitable PID controller parameters, the noise suppression in the low-frequency domain could be enhanced, which is of interest for applications that require long-term stability of the magnetic field [7].

V. DISCUSSION AND CONCLUSION

We report a dual-species all-optical magnetometer based on a paraffin-coated Cs-K hybrid vapor cell. Using the amplitude-modulated Bell-Bloom scheme and Faraday-rotation measurement, we show that the spin polarization of Cs and K atoms can be generated and detected independently. The proposed design could be applied in active magnetic field stabilization or current-source-noise stabilization [7,17]. In these applications, despite the use of high-sensitivity optically pumped magnetometers, it is still difficult to characterize the practical noise after stabilization in the presence of magnetic field gradients. Active magnetic field stabilization based on *in situ* measurement can promote an accurate evaluation of the degree of noise suppression, while the influence of magnetic field gradients could be eliminated.

The proposed scheme could also be applied in a practical ground-surveying magnetometer based on dual working species. It should be noted the K magnetic resonance spectrum splits into separate lines in the range of the terrestrial magnetic field, which is smaller in signal amplitude than an entirely overlapped line under a small magnetic field, indicating that the intrinsic sensitivity of the K channel under the terrestrial magnetic field will be lower than the test results reported in Sec. III A. However, the K channel still potentially offers higher sensitivity in the range of large terrestrial magnetic fields (typically more than 50 μT), where the sensitivity of the Cs channel would decrease under the influence of the nonlinear Zeeman effect [6,39]. Considering the high cost of four independent lasers, an improvement could be considered to reduce the use of lasers; for example, a single-beam Bell-Bloom scheme could be used to generate and detect the atomic spins of each species [48].

A method to improve further the performance of the K channel in our scheme involves designing a hybrid vapor cell in which the atomic densities of the Cs atoms and the K atoms could be controlled individually [11], and thus the Cs atomic density could be kept relatively low to decrease the SE collisions experienced by the K atoms, thereby suppressing the K-magnetic-resonance-broadening effect. In addition, we also hope to study the light-narrowing effect since achieving a high atomic polarization through efficient optical pumping is another way to suppress SE broadening under a high field [49–52].

[1] I. K. Kominis, T. W. Kornack, J. C. Allred, and M. V. Romalis, A subfemtotesla multichannel atomic magnetometer, Nature **422,** 596 (2003).

[2] D. Sheng, S. Li, N. Dural, and M. V. Romalis, Sub-femtotesla Scalar Atomic Magnetometry Using Multipass Cells, Phys. Rev. Lett. **110,** 160802 (2013).

[3] E. B. Aleksandrov, Advances in quantum magnetometry for geomagnetic research, Phys.-Usp. **53,** 509 (2010).

[4] V. Y. Shifrin, E. B. Alexandrov, T. I. Chikvadze, V. N. Kalabin, V. N. Yakobson, V. N. Khorev, and P. G. Park, Magnetic flux density standard for geomagnetometers, Metrologia **37,** 219 (2000).

[5] E. B. Aleksandrov, Precision atomic-resonance magnetometers for geomagnetic measurements, Meas. Tech. **28,** 312 (1985).

[6] Y. Ding, R. Zhang, J. Zheng, J. Chen, X. Peng, T. Wu, and H. Guo, Active stabilization of terrestrial magnetic field with potassium atomic magnetometer, Rev. Sci. Instrum. **93,** 015003 (2022).

[7] R. Zhang, Y. Ding, Y. Yang, Z. Zheng, J. Chen, X. Peng, T. Wu, and H. Guo, Active magnetic-field stabilization with atomic magnetometer, Sensors **20,** 4241 (2020).

[8] C. P. Hao, Q. Q. Yu, C. Q. Yuan, S. Q. Liu, and D. Sheng, Herriott-cavity-assisted closed-loop Xe isotope comagnetometer, Phys. Rev. A **103,** 053523 (2021).

[9] T. W. Kornack, R. K. Ghosh, and M. V. Romalis, Nuclear Spin Gyroscope Based on an Atomic Comagnetometer, Phys. Rev. Lett. **95,** 230801 (2005).

[10] E. B. Alexandrov, M. V. Balabas, A. K. Vershovski, and A. S. Pazgalev, Experimental demonstration of the sensitivity of an optically pumped quantum magnetometer, Tech. Phys. **49,** 779 (2004).

[11] E. B. Aleksandrov, M. V. Balabas, A. K. Vershovskii, and A. S. Pazgalev, A new model of a quantum magnetometer: A single-cell Cs-K tandem based on four-quantum resonance in ³⁹K atoms, Tech. Phys. **45,** 931 (2000).

[12] D. F. Kimball, I. Lacey, J. Valdez, J. Swiatlowski, C. Rios, R. Peregrina-Ramirez, C. Montcrieffe, J. Kremer, J. Dudley, and C. Sanchez, A dual-isotope rubidium comagnetometer to search for anomalous long-range spin-mass (spin-gravity) couplings of the proton, Ann. Phys. **525,** 514 (2013).

[13] S. Groeger, G. Bison, P. E. Knowles, R. Wynands, and A. Weis, Laser-pumped cesium magnetometers for

high-resolution medical and fundamental research, Sens. Actuators A Phys. **129**, 1 (2006).

[14] K. Libbrecht and J. L. Hall, A low-noise high-speed diode laser current controller, Rev. Sci. Instrum. **64**, 2133 (1993).

[15] C. Y. Wu, W. M. Chen, and L. T. Kuo, A CMOS power-efficient low-noise current-mode front-end amplifier for neural signal recording, IEEE Trans. Biomed. Circuits Syst. **7**, 107 (2013).

[16] E. B. Aleksandrov, M. V. Balabas, S. P. Dmitriev, N. A. Dovator, A. I. Ivanov, I. A. Krasnoshchekova, V. N. Kulyasov, V. V. Marchenkov, A. S. Pazgalev, and A. P. Serebrov, Gradiometric investigation of a cesium-vapor quantum magnetometer, Tech. Phys. **52**, 389 (2007).

[17] L. Shen, R. Zhang, T. Wu, X. Peng, S. Yu, J. Chen, and H. Guo, Suppression of current source noise with an atomic magnetometer, Rev. Sci. Instrum. **91**, 084701 (2020).

[18] W. Happer and A. C. Tam, Effect of rapid spin exchange on the magnetic-resonance spectrum of alkali vapors, Phys. Rev. A **16**, 1877 (1977).

[19] J. C. Allred, R. N. Lyman, T. W. Kornack, and M. V. Romalis, High-Sensitivity Atomic Magnetometer Unaffected by Spin-Exchange Relaxation, Phys. Rev. Lett. **89**, 130801 (2002).

[20] R. K. Ghosh and M. V. Romalis, Measurement of spin-exchange and relaxation parameters for polarizing ^{21}Ne with K and Rb, Phys. Rev. A **81**, 043415 (2010).

[21] W. Li, X. Peng, D. Budker, A. Wickenbrock, B. Pang, R. Zhang, and H. Guo, Hybrid optical pumping of K and Rb atoms in a paraffin coated vapor cell, Opt. Lett. **42**, 4163 (2017).

[22] J. Skalla, G. Wackerle, and M. Mehring, Coherence transfer between atomic transitions of different *g*-factor by modulated optical excitation, Opt. Commun. **127**, 31 (1996).

[23] Y. Ito, H. Ohnishi, K. Kamada, and T. Kobayashi, Development of an optically pumped atomic magnetometer using a K-Rb hybrid cell and its application to magnetocardiography, AIP Adv. **2**, 032127 (2012).

[24] M. V. Romalis, Hybrid Optical Pumping of Optically Dense Alkali-Metal Vapor without Quenching Gas, Phys. Rev. Lett. **105**, 243001 (2010).

[25] S. J. Seltzer, Developments in alkali-metal atomic magnetometry, Dissertation, Princeton University (2008).

[26] O. Katz, O. Peleg, and O. Firstenberg, Coherent Coupling of Alkali Atoms by Random Collisions, Phys. Rev. Lett. **115**, 113003 (2015).

[27] W. E. Bell and A. L. Bloom, Optically Driven Spin Precession, Phys. Rev. Lett. **6**, 280 (1961).

[28] G. Bevilacqua, V. Biancalana, Y. Dancheva, A. Fregosi, and A. Vigilante, Spin dynamic response to a time dependent field, Appl. Phys. B **127**, 128 (2021).

[29] R. Zhang, W. Teng, J. Chen, X. Peng, and H. Guo, Frequency response of optically pumped magnetometer with nonlinear Zeeman effect, Appl. Sci. **10**, 7031 (2020).

[30] R. Zhang, B. Pang, Y. Li, W. Yang, J. Chen, X. Peng, and H. Guo, in *Proceedings of the 2018 IEEE International Frequency Control Symposium* (IEEE, Olympic Valley, CA, USA, 2018), p. 21.

[31] G. Bevilacqua, V. Biancalana, Y. Dancheva, and A. Vigilante, Self-adaptive loop for external-disturbance reduction in a differential measurement setup, Phys. Rev. Appl. **11**, 014029 (2019).

[32] R. Zhang, W. Xiao, Y. Ding, Y. Feng, X. Peng, L. Shen, C. Sun, T. Wu, Y. Wu, Y. Yang, Z. Zheng, X. Zhang, J. Chen, and H. Guo, Recording brain activities in unshielded Earth's field with optically pumped atomic magnetometers, Sci. Adv. **6**, aba8792 (2020).

[33] W. Xiao, T. Wu, X. Peng, and H. Guo, Atomic spin-exchange collisions in magnetic fields, Phys. Rev. A **103**, 043116 (2021).

[34] C. B. Alcock, V. P. Itkin, and M. K. Horrigan, Vapour pressure equations for the metallic elements: 298–2500 K, Can. Metall. Q. **23**, 309 (1984).

[35] S. Appelt, A. Baranga, C. J. Erickson, M. V. Romalis, A. R. Young, and W. Happer, Theory of spin-exchange optical pumping of ^{3}He and ^{129}Xe, Phys. Rev. A **58**, 1412 (1998).

[36] See Supplemental Material http://link.aps.org/supplemental/10.1103/PhysRevApplied.19.034066 for a more-detailed derivation of magnetic resonance broadening and polarization transfer in the K-Cs hybrid ensembles.

[37] V. A. Kartoshkin, Spin-exchange processes in a single-chamber Cs-K tandem magnetometer, Opt. Sepctrosc. **113**, 235 (2012).

[38] N. W. Ressler, R. H. Sands, and T. E. Stark, Measurement of spin-exchange cross sections for ^{133}Cs, ^{87}Rb, ^{85}Rb, ^{39}K, and ^{23}Na, Phys. Rev. **184**, 102 (1969).

[39] E. B. Aleksandrov and A. K. Vershovskii, Modern radio-optical methods in quantum magnetometry, Phys.-Usp. **52**, 573 (2009).

[40] T. Ito, N. Shimomura, and T. Yabuzaki, Transfer of precessing spin polarizations between different kinds of atoms with same *g*-factor, J. Phys. Soc. Jpn. **72**, 1302 (2003).

[41] F. Bloch, Nuclear induction, Phys. Rev. **70**, 460 (1946).

[42] T. W. Kornack, A test of CPT and Lorentz symmetry using a K-^{3}He co-magnetometer, Dissertation, Princeton University (2005).

[43] E. V. Blinov, R. A. Zhitnikov, E. A. Ilin, P. P. Kuleshov, and V. Y. Shifrin, Metrological analysis of alkali-helium magnetometers, Meas. Tech. **29**, 1078 (1986).

[44] H. Ito, T. Ito, and T. Yabuzaki, Accumulative transfer of transverse magnetic moment between spin-locked Rb and Cs atoms, J. Phys. Soc. Jpn. **63**, 1337 (1994).

[45] Y. Ito, H. Ohnishi, K. Kamada, and T. Kobayashi, Sensitivity improvement of spin-exchange relaxation free atomic magnetometers by hybrid optical pumping of potassium and rubidium, IEEE Trans. Magn. **47**, 3550 (2011).

[46] A. B. Baranga, A. Stephan, M. V. Romalis, C. Erickson, A. Young, G. Cates, and W. Happer, Polarization of ^{3}He by Spin Exchange with Optically Pumped Rb and K Vapors, Phys. Rev. Lett. **80**, 2801 (1998).

[47] W. C. Chen, T. R. Gentile, T. G. Walker, and E. Babcock, Spin-exchange optical pumping of ^{3}He with Rb-K mixtures and pure K, Phys. Rev. A **75**, 013416 (2007).

[48] M. Petrenko, A. Pazgalev, and A. Vershovskii, Single-Beam All-Optical Nonzero-Field Magnetometric Sensor for Magnetoencephalography Applications, Phys. Rev. Appl. **15**, 064072 (2021).

[49] N. D. Bhaskar, J. Camparo, W. Happer, and A. Sharma, Light narrowing of magnetic resonance lines in dense, optically pumped alkali-metal vapor, Phys. Rev. A **23**, 3048 (1981).

[50] S. Appelt, B. A. Baranga, A. R. Young, and W. Happer, Light narrowing of rubidium magnetic-resonance lines in high-pressure optical-pumping cells, Phys. Rev. A **59,** 2078 (1999).

[51] B. Julsgaard, J. Sherson, J. L. Rensen, and E. S. Polzik, Characterizing the spin state of an atomic ensemble using the magneto-optical resonance method, J. Opt. B Quantum Semiclass. Opt. **6,** 5 (2003).

[52] T. Scholtes, V. Schultze, R. Ijsselsteijn, S. Woetzel, and H. G. Meyer, Light-narrowed optically pumped M_x magnetometer with a miniaturized Cs cell, Phys. Rev. A **84,** 043416 (2011).